Magnetic Resonance in Medicine 49:158–167 (2003)

# Multiple-Mouse MRI

Nicholas A. Bock,[1–3]* Norman B. Konyer,[2] and R. Mark Henkelman[1–3]

**Several theoretical parallel-imaging approaches are evaluated that seek to improve the efficiency of an MRI experiment involving multiple small samples, such as mice. The best method for our mouse phenotyping application is chosen in terms of efficiency and ease of implementation, and the approach is demonstrated at 1.5 T on a clinical scanner with an array of four shielded birdcage coils with four parallel receivers. Electronic interactions between the receiver channels in the system are quantified and a novel sensitivity-encoding (SENSE)-like postprocessing method is described to remove the resulting image ghosts. In parallel imaging with a four-coil array, the time required for three-dimensional (3D) high-resolution imaging of four mice is reduced to one-fourth the time that it would take to image the mice sequentially. Magn Reson Med 49:158–167, 2003. © 2003 Wiley-Liss, Inc.**

**Key words: MRI; parallel imaging; mouse imaging; coil array; SENSE**

A new era of discovery issues from the mapping of the human genome, and the functions of these genes must now be found. Because of the strong homology between human and other mammalian genes, it is expected that many human gene functions will be inferred from those in animals, particularly mice. To facilitate such postgenomics work in mice, a number of large-scale, genome-wide mutagenesis programs have been started (1,2). The ultimate goal of these programs is to produce at least one heritable mutation in every gene in the mouse genome and to assign at least one function to the mutation. To so relate mutation to function requires a return to a classic genetics approach that thoroughly investigates the phenotype of each mutant mouse.

One important screening method for finding unknown phenotypes is whole-body, high-resolution, three-dimensional (3D) imaging of anatomy, preferably using an in vivo modality that allows for subsequent research using the living animal. Since a 3D image may be viewed from different orientations, suspected abnormalities can be viewed in whichever plane is best suited to the anatomy. For visual inspection of fewer slices, isotropic data can be averaged perpendicular to the image plane. The merits of screening fixed specimens and perfused organs with 3D isotropic resolution have also been demonstrated (3). MRI is ideal because it is both nondestructive and 3D. It also avoids many of the drawbacks of serial sectioning (which is the current gold standard for anatomical studies), such as dissection of the sample, distortion and misalignment of slices during computer registration, and difficulty in automation (4). An MRI screen could detect structural abnormalities in a suspected mutant mouse by comparing a high-resolution (50 μm) 3D isotropic image of it to an image of a reference mouse using computer registration and analysis. The utility of such registration programs depends on high image quality (5) and hence long imaging times, since signal-to-noise ratio (SNR), resolution, and contrast all dictate increased acquisition times in MRI. Notwithstanding the recent efforts in designing radiofrequency (RF) coils and pulse sequences to increase MRI's sensitivity for use in microscopic studies of mice, whole-body scans at high fields still require long imaging times. In a recent study at 7 T, 100 × 100 × 100 μm whole-body mouse imaging took 14 hr (6). Such long imaging times are prohibitive; the phenotypic screening of dominant genes alone is likely to require at least 20000 animals (7). Thus, in order to realize the value of MRI as an effective means of phenotyping mice, ways to improve its efficiency must be developed. A similar approach to increase the throughput in NMR spectroscopy studies has already been addressed (8,9), but in the present work we focus on increasing throughput in an MRI study.

Instead of trying to reduce the imaging time for each mouse by further increasing the sensitivity of MRI, we propose to reduce the overall time needed to image a large number of mice. If several mice are imaged in the same scanner in parallel, then the length of imaging time required per mouse can be reduced. The work is motivated by our plans to image multiple mice in a 7 T scanner for a mouse mutagenesis screening program. We demonstrate that imaging mice in separate shielded RF coils in a common magnet and gradient coil can effectively improve efficiency in whole-body anatomical screening of mice. This technique can also increase the throughput in other animal screening methods, such as those used in the pharmaceutical industry to screen animal responses. However, in studies in which the specific location of the abnormality is known, a two-dimensional (2D) imaging sequence used with our technique may be preferable to a whole-body 3D imaging sequence. Finally, our technique could be used to reduce the overall imaging time needed in clinical bilateral studies, such as wrist or leg imaging (10), wherein anatomical regions can be imaged in completely isolated RF coils.

## THEORY

### Approaches for Paralleling

To increase the throughput of a scanner being used in a mouse-screening program, we need to consider ways of improving efficiency. One intuitive, albeit expensive, way to increase the efficiency in a multiple-mouse experiment

[1]Department of Medical Biophysics, University of Toronto, Toronto, Canada.
[2]Sunnybrook and Women's College Health Sciences Center, Toronto, Canada.
[3]Mouse Imaging Center (MICE), Hospital for Sick Children, Toronto, Canada.
*Correspondence to: Nicholas Bock, Room S605, Imaging Research, Sunnybrook and Women's College Health Sciences Center, 2075 Bayview Ave., Toronto, Ontario M4N 3M5, Canada. E-mail: nbock@sten.sunnybrook.utoronto.ca

Received 30 January 2002; revised 14 August 2002; accepted 20 August 2002.
DOI 10.1002/mrm.10326
Published online in Wiley InterScience (www.interscience.wiley.com).

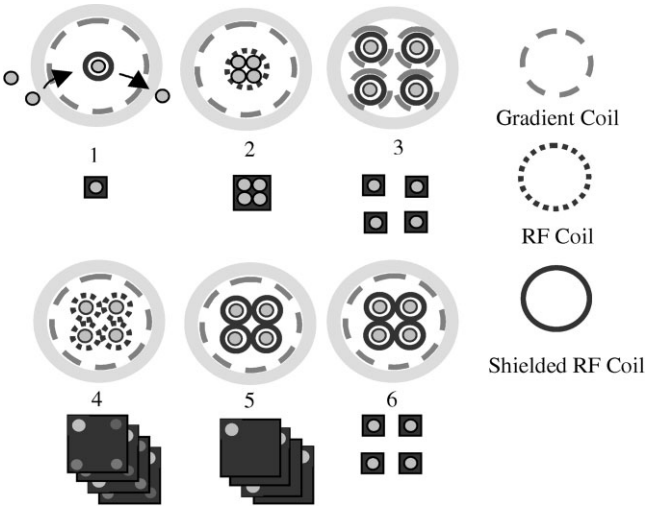


FIG. 1. Six approaches to multiple-mouse imaging in a single magnet bore. The image(s) produced in each case are shown below their respective equipment setup.

is to run many scanners in parallel. Fortunately, one can approach similar efficiency at a much lower cost by making discriminating changes in the arrangement of the gradient and RF coils in the bore of a single high-field magnet.

Several approaches to multiple-mouse imaging are presented and evaluated in Fig. 1 and Table 1. The ultimate goal of each approach is to produce identical high-resolution, whole-body 3D images of a large number of mice in the most efficient manner possible. Each mouse can be mechanically positioned in the scanner, or a scout sequence can be used to define the 3D volume for imaging prior to each scan. The first approach images each mouse in turn in a small-animal RF coil and gradient coil, with an FOV covering that mouse. The second approach images several mice at once in a single RF coil and gradient coil, with an FOV covering all of the mice (11). The third approach images mice in separate RF coils with separate receivers and gradient coils in a common magnet, with FOVs covering each mouse (12). The fourth approach images mice in separate unshielded RF coils on separate receivers in a common gradient coil and magnet, with an FOV covering all of the mice. The fifth approach images mice in separate shielded RF coils with separate receivers in a common gradient coil and magnet, with an FOV covering all of the mice (13), or, in the sixth approach, with the FOV reduced so that it covers only one mouse (14).

Table 1
A Comparison Between the Six Cases of Minimum Imaging Time, SNR Normalized to Case 1, and SNR Efficiency

| Case | Minimum imaging time for *N* mice | SNR in each mouse image normalized to Case 1 | SNR efficiency |
|---|---|---|---|
| 1 | *Nt* | 1 | 1 |
| 2 | *Nt* | 1 | 1 |
| 3 | *t* | 1 | *N* |
| 4 | $\alpha Nt$ | $\alpha^{1/2}$ to $(\alpha N)^{1/2}$ | 1 to *N* |
| 5 | $\alpha Nt$ | $(\alpha N)^{1/2}$ | *N* |
| 6 | *t* | 1 | *N* |

*N*, number of mice; *t*, time for a single mouse to be imaged in Case 1; $\alpha$, increase in FOV area to cover *N* mice with RF coils.

For each of these cases, a comparison of SNR and efficiency is made (Table 1) based on several assumptions. It is assumed that sample noise is dominating and that in cases 3, 5, and 6 completely shielded transmit/receive RF coils are used that are electrically independent. The coils could be birdcage coils, solenoid coils, or any other type of volume coil capable of transmitting. The coils should be matched in size to the mice to increase sensitivity. We also assume that in each case, the same optimized 3D pulse sequence images the mice with the readout gradient oriented along their long axes and the phase-encoding gradients across the face of the array of mice. For cases with multiple mice in the magnet at one time, we assume that they are laid out in a grid array, although in reality, one might want to use a different packing geometry to improve efficiency. In our example, the time that the pulse sequence requires is directly proportional to the number of phase encodes needed to produce the FOV area. The SNR the sequence produces is proportional to the square root of the number of phase encodes. Thus, the only imaging parameter that is changed between cases is the FOV, and an increase in the area of the FOV by a factor of *N* across the face of the array will increase the imaging time by a factor of *N* and increase the SNR by a factor of $N^{1/2}$. Therefore, two important criteria for comparisons between cases shown in Table 1 are: *1* the minimum time required to image *N* mice with the pulse sequence, and *2* the resultant SNR that would be produced in each image.

If we take the ratio of the time needed to produce the SNR of case 1 by the time needed to produce that SNR in another case, we can define the SNR efficiency of each case. In three of the cases, the efficiency is not dependent on the number of mice being imaged, although it will be limited by the number of mice that can fit in the bore of the scanner at once; hence, packing is also a criterion for comparison. Finally, the simplicity of each case must be considered, since cases with equal efficiencies differ in the equipment requirements and the complexity of the experimental implementation.

Case 1 is a reference case in which a dedicated animal scanner is used to image *N* mice in turn. If in case 1 it takes time *t* to image a mouse with an SNR of $\Psi$, then *N* mice will take *Nt* units of time to image with an SNR of $\Psi$ in each resultant image, and the SNR efficiency will be one. This is the simplest case, presented as a reference, and packing is not a consideration because only one mouse is in the bore of the magnet at a time.

In case 2, several mice are imaged either together in a single coil, such as a knee or head coil, or in an array of mouse-sized coils that are input to a common receiver. While case 2 may appear to improve efficiency when sample noise dominates, no improvement is in fact achieved. The classic discussion of SNR in an MR experiment derives from the following expression (15):

$$\Psi \propto \frac{\nu^2 B_1}{(r_{coil} + r_{sample})^{1/2}} \propto \frac{\nu^2 B_1}{[\alpha \nu^{1/2} + \beta B_1 \nu^2]^{1/2}} \qquad [1]$$

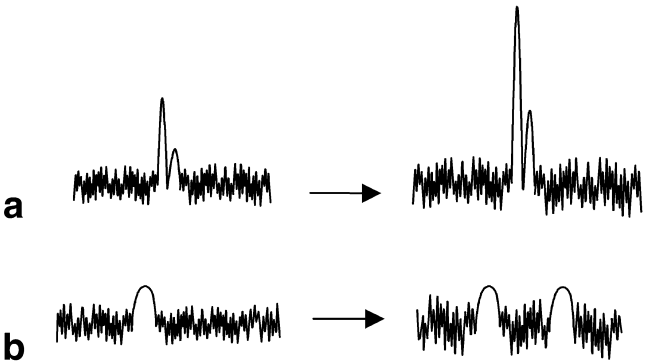


FIG. 2. Signal acquisition with one mouse and two mice in the RF coil (**a**) with no gradients and (**b**) with a gradient. In the case with no gradients, the signal increases by a factor of 2, while the noise increases by $2^{1/2}$. However, when the signals are separated in frequency space with a gradient, the local signal amplitude does not increase, while the noise still increases by a factor of $2^{1/2}$.

The first term in the denominator represents the noise from RF coil resistance, and the second term is the noise from losses in the sample. The $\alpha$ and $\beta$ terms are constant for a given coil and sample size, $\nu$ is the frequency, and $B_1$ is the strength of the RF field produced by the coil carrying unit current. Thus, we can consider two imaging extremes in case 2: one in which coil noise dominates, and one in which sample noise dominates. In reality, mouse imaging falls between those two noise extremes, depending on the field strength at which it is performed.

In considering the efficiency of case 2 when sample noise dominates, the SNR should be determined from the resultant images rather than the unprocessed signal. Compare a gradientless acquisition when sample noise dominates with a single mouse in a coil to the same acquisition with $N$ mice in that coil (in the figure, $N = 2$) (Fig. 2a). With the increase to $N$ mice, the signal increases in amplitude by a factor of $N$, while the noise only increases by a factor of $N^{1/2}$. Thus, the SNR gain in the signal is $N^{1/2}$. When the signals are separated in frequency space with a gradient, however, the local signals (which are what we would use to calculate SNR in an image) are constant in amplitude regardless of the number of mice, but the noise still increases by a factor of $N^{1/2}$ (Fig. 2b). Therefore, the SNR in the image actually decreases as $N^{1/2}$.

To image $N$ mice, however, the FOV area must increase by a factor of $N$; hence, the imaging time increases by a factor of $N$ and a factor of $N^{1/2}$ is regained in the SNR. This means that imaging $N$ mice will take $Nt$ units of time with a final SNR of $\Psi$, and that case 2 has the same SNR efficiency as case 1. The packing of the mice is best in case 2, but since the efficiency remains the same as case 1 regardless of how many mice are placed in the bore at once, no efficiency gain is realized.

Conversely, if coil noise dominates, then the geometry of the coil used in case 2 will affect the overall efficiency. For comparison, however, we will assume that $N$ coils with identical geometric factors to the coil used in case 1 are input to the receiver. The $B_1$ sensitivities of the coils will be the same as in case 1, so that the only parameter that changes in Eq. [1] between the cases is the coil noise. That noise increases by a factor of $N^{1/2}$, since we now have incoherent noise from $N$ coils, although we are again imaging for $N$ times longer, so our final SNR is still $\Psi$. Thus, the SNR efficiency is the same as when sample noise dominates in case 2, as shown in Table 1. Although in case 2 there is no gain in SNR efficiency, there may be a gain in throughput efficiency over the entire experiment if imaging multiple mice reduces the overall number of scout and shimming scans that need to be performed.

In case 3, the mice share a common static magnetic field, but have distinct and electrically isolated RF coils, receiver channels, and gradient coils so that each mouse can be imaged independently of its neighbors. The signal transmitted to each coil could come from a single transmitter split $N$ ways, or from $N$ separate transmitters. Thus, $N$ mice can be imaged concurrently in the same magnet, each with an SNR of $\Psi$ in $t$ units of time, which is the same efficiency as $N$ scanners operating in parallel. Imaging more mice concurrently will not increase the minimum imaging time, although efficiency will ultimately be limited by the number of gradient coils that can fit in the bore of the magnet. Case 3 has a poor packing density because each mouse has its own RF coil and gradient set. This case is also the most complicated in terms of equipment, because of the $N$ separate gradient sets that need to be driven independently. However, there is a benefit in using case 3 when magnet homogeneity must be maximized: the ability to use each mouse's gradients for first-order shimming makes case 3 preferable in studies in which water/fat suppression is required, for gradient-echo imaging, and for spectroscopic imaging studies. In the other cases, the mice would have to be shimmed as a single volume, meaning that magnet homogeneity would not be as good as when a single mouse is shimmed.

In case 4, unshielded RF coils on separate receivers are used to image the mice in a common gradient coil. Case 4 also represents imaging multiple mice with a phased-array coil. Thus, the noise in each image depends on the amount of coupling between the coils and the sensitivity of each coil to the mice in other coils. In the worst noise case, in which the coils are completely coupled, the minimum imaging time is $\alpha N$ (where $\alpha$ is an extra factor multiplying the FOV area to accommodate the RF coils), the SNR in the final images is $\alpha^{1/2}\Psi$, and the SNR efficiency is one (the same as in case 2). In the best case, the coils are completely isolated, so that the amount of noise and the signal amplitude in any image are independent of the number of mice being imaged. Thus, the minimum imaging time is $\alpha Nt$, the resultant SNR is $(\alpha N)^{1/2}\Psi$, and the SNR efficiency is $N$. In reality, the coupling will fall somewhere in between these limits, although complete isolation can be achieved by shielding the RF coils.

In cases 5 and 6, each mouse is imaged in a distinct and isolated RF coil with its own receiver channel inside a common gradient coil and magnet. Again, the transmit signals could come from a single split transmitter or from separate transmitters. In case 5, the FOV is set over the entire array of mice; in that regard, it is identical to the extreme of case 4 in which there is no interaction between the RF coils. Because the RF coils are shielded and have their own receivers, both the signal amplitude and the amount of noise in any image are independent of the

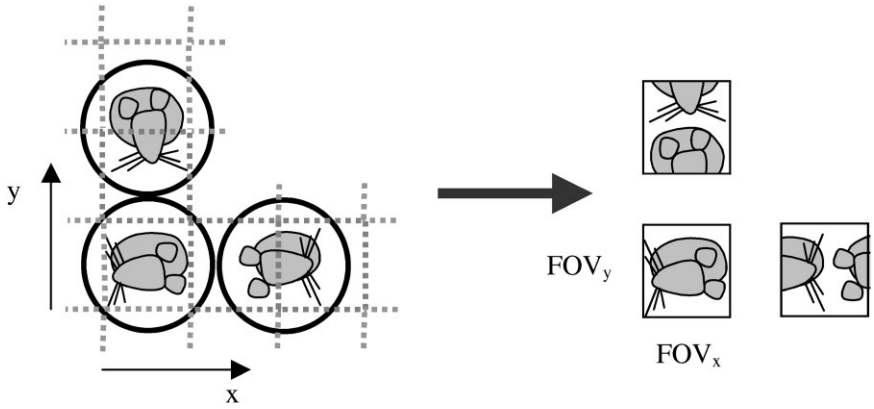


FIG. 3. The FOV applied to one mouse in case 6 is replicated over the other mice in the array. Mice that were not centered in an FOV will appear shifted in the final images, but can be centered in postprocessing by an appropriate choice of origin.

number of mice being imaged. In imaging $N$ mice, the FOV must be increased by a factor of $\alpha N$. This means that the imaging time increases by a factor of $\alpha N$; hence, the resultant SNR gain in the images is $(\alpha N)^{1/2}\Psi$. Even though the minimum imaging time is longer than in cases 1 and 2, the images have a significantly higher SNR; in fact, the SNR efficiency is $N$, which is the same as for case 3. The packing is better than in case 3 and the experiment is also less complicated.

In case 6, a subtle change is made in the imaging sequence that trades SNR for a reduction in the minimum imaging time for $N$ mice. The FOV is reduced to cover only one mouse in the array, and the other mice are spatially encoded by replicated FOVs in the phase-encoding directions. If the mice were not in shielded RF coils, the images of the separate mice would fold over each other. Because each RF coil and receiver channel is only sensitive to its own mouse, however, there is no superposition of the individual mouse signals. Thus, imaging $N$ mice with an SNR of $\Psi$ takes $t$ units of time—once again, the same efficiency obtained by running $N$ scanners in parallel. One complication is that some mice are not centered in a replicated FOV, so postprocessing is required to correct for phase offsets in those images by multiplying the raw $k$-space data by a factor of $\exp(-i2\pi(k_x x + k_y y))$, where $x$ and $y$ are the displacements of the mouse in the array (Fig. 3). It should be noted that when coil isolation is not complete and the coils couple, cases 3, 5, and 6 can be considered as case 4 (the case in which unshielded coils are used). It should also be noted that case 6 can also be used with 2D sequences. With a 2D sequence, the slice-select gradient is used to excite a slice that is in all of the mice. Then the phase-encoding and readout FOVs are reduced to cover just one mouse in the array. The frequency offsets of the anti-aliasing filters on the readout A/D converters must be matched to the position of each mouse, but reducing the readout FOV reduces bandwidth and the size of the image data set that is collected, thus reducing total time.

As summarized in Table 1, cases 3, 5, and 6 have the best efficiencies, although cases 5 and 6 are preferable because the packing is better than in case 3, in which separate gradient coils are needed for each RF coil. Case 6 is ultimately the best method for 3D, high-resolution, multiple-mouse imaging because it also achieves the shortest minimum imaging time.

For more complicated investigations, such as cardiac imaging, case 6 may not be preferable. While one could collect a cardiac and respiratory signal from each mouse and reorder the phase-encoding data after imaging, gating would not be possible because it would require the coincidence of the cardiac and respiratory cycles of all of the mice. In those situations, case 1 or 3 would be preferable.

## Packing of Multiple Shielded Coils

Based on those considerations, we are planning to implement case 6 to image multiple mice in a 7 T, 40-cm clear-bore scanner. Although we will only have four receiver channels on our scanner, we plan to image with 16 RF coils using a multiplexing scheme (16) similar to multislab 3D imaging. We will apply an RF excitation in a fast spin-echo sequence to a group of four coils using a common transmitter, a slab-select gradient, and four separate receivers. During the pulse repetition time (TR) for those coils, an identical RF excitation will be applied to the next group of four coils by switching the transmitter and the receivers to them. Provided that an acquisition from each of the groups of coils can be accomplished during the TR for the first group, and that TR is less than $T_1$, efficiency will not be compromised.

The number of RF coils possible in any array will depend on the available space in the bore of the gradient and on the number of parallel or multiplexed receiver channels on the scanner. Since the mice need to be loaded into the coils from the front of the magnet, and anesthetized from the back, only one layer of coils can be easily handled within the bore. Birdcage coils best suit this geometry. While there may be an increase in SNR using solenoidal coils, they would have to be placed sideways in the bore of the magnet and the entire array would have to be removed each time to change the mice. The optimum array geometry for a layer of cylindrical coils can be observed in the solutions of the dense packing of congruent circles within a larger circle (17). Since the number of receiver channels on future scanners will likely increase, Fig. 4a shows several optimal geometries for even numbers of coils, and Fig. 4b plots the diameter of the bore against the number of coils.

In our array, we will only have 16 active coils, but we are designing a hexagonal array (dubbed *Mousehive*) with three extra coils in it to minimize the down time should one of the coils fail. In addition, since cylinders naturally pack closely in that geometry, it is simpler to construct. Because the hexagonal packing of the 19 coils is denser

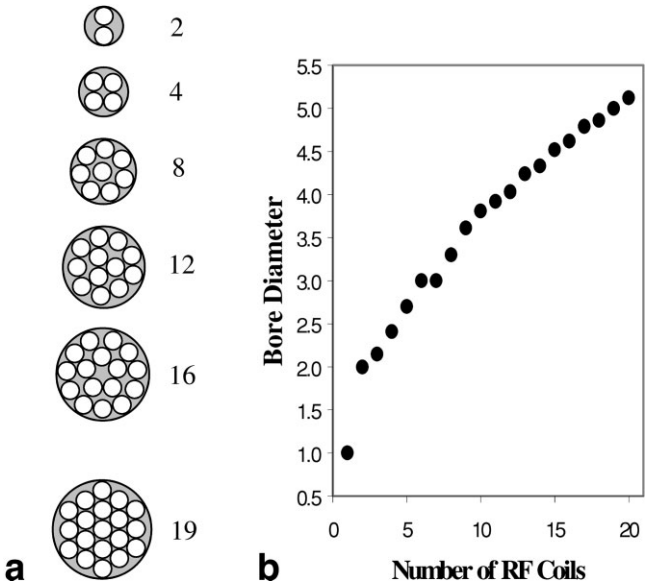


FIG. 4. **a:** Optimum packing geometries for cylindrical RF coils in a magnet bore, and *Mousehive*, a close-packed hexagonal arrangement of 19 RF coils. **b:** Plot of the bore diameter (in units of RF coil diameters) required for a given number of RF coils.

than the optimum configuration of 16 coils, the addition of three spare coils increases our required gradient bore diameter by only 0.4 RF coil diameters.

More mouse RF coils can fit in the bore of the gradient if the RF shield diameter decreases. However, there is a decrease in RF coil $B_1$ strength with a decreasing shield diameter/RF coil diameter ratio (18) that limits the diameter of the shields used. Since the mean shield diameter/coil diameter ratio for a hexagonal shield is greater than for a cylindrical shield that takes up the same space in our array, we have investigated a potential SNR advantage in using hexagonal shields.

### Correcting for Ghosts

So far, we have considered RF coils and receiver channels that are electromagnetically isolated. The situation becomes more complicated, however, if that isolation is not complete. Isolation between two channels on the scanner can be compromised in two ways. If the shielding on the RF coils is incomplete, a coil may inductively couple to another coil and the mouse within it. There may also be reactive coupling between the cables and electronics of separate receiver channels. Those couplings will have two effects: ghost images of mice will appear in the images of other mice, and the noise in the images will increase.

Regardless of the mechanism of coupling used, we can use the sensitivity-encoding (SENSE) theory (19) to correct the ghosted images and to analyze the noise in those corrected images. Following the theory developed by Pruessmann et al. (19), consider one pixel location in an image with overlapped ghosts. Let $N$ denote the number of mice being imaged and assemble in the vector **a** the complex image values the chosen pixel has in the $N$ overlapping images. If $S_{i,j}$ is the complex sensitivity of the $i^{\text{th}}$ RF coil or receiver channel to the $j^{\text{th}}$ superimposed pixel, then we can write

$$\mathbf{v} = S_{i,j}^{-1}\mathbf{a} \qquad [2]$$

where **v** is a vector of length $N$ that lists the separated values of the originally superimposed pixels. Separated images can be obtained by repeating Eq. [2] for every pixel position in the overlapped images. In the case of inadequate RF coil shielding, the experimental method from SENSE must be followed and the sensitivity matrix $S_{i,j}$ for each pixel determined by accurately mapping local coil sensitivities. If the ghosting is caused by electronic coupling in the receiver channels, however, a simpler method may be used, whereby the matrix $S_{i,j}$ is the same for all pixels in the overlapped image and can be measured by determining the sensitivity of each receiver channel to a signal placed in turn on the other channels.

While the elimination of ghosts can be achieved in both cases, it is important to note that the mechanism of coupling will affect the amount of noise in the corrected images. Consider signal separation in the case of two mice

$$\mathrm{a} = \begin{bmatrix} \mathrm{A}_1 \\ \mathrm{A}_2 \end{bmatrix} \qquad [3]$$

where $A_1$ and $A_2$ are the complex pixel values measured in the first and second folded mouse images. In reality, those values will be the sum of the actual pixel values, $V_1$ and $V_2$, weighted by complex sensitivities, and the noise, $N$, in the folded pixel. Thus, we can write

$$S_{i,j}^{-1}\mathrm{a} = S_{i,j}^{-1}\begin{bmatrix} S_{11}V_1 + S_{12}V_2 + N_1 \\ S_{21}V_1 + S_{22}V_2 + N_2 \end{bmatrix} = \mathrm{v} + S_{i,j}^{-1}\begin{bmatrix} N_1 \\ N_2 \end{bmatrix}. \qquad [4]$$

In the complete SENSE case, the first RF channel detects noise from its coil ($N_{11\text{coil}}$) , its mouse ($N_{11\text{mouse}}$), and its preamplifier ($N_{1\text{preamp}}$) as well as noise from the second coil ($N_{12\text{coil}}$) and its mouse ($N_{12\text{mouse}}$). A similar combination of noises appears in the second channel as well so that

$$\begin{bmatrix} N_1 \\ N_2 \end{bmatrix} = \begin{bmatrix} N_{11coil} + N_{11mouse} + N_{12coil} + N_{12mouse} + N_{1preamp} \\ N_{21coil} + N_{21mouse} + N_{22coil} + N_{22mouse} + N_{2preamp} \end{bmatrix}. \qquad [5]$$

This means that signal separation with Eq. [4] yields

$$S_{i,j}^{-1}a = \mathrm{v} + S_{i,j}^{-1}\begin{bmatrix} N_{11coil} + N_{11mouse} + N_{12coil} + N_{12mouse} + N_{1preamp} \\ N_{21coil} + N_{21mouse} + N_{22coil} + N_{22mouse} + N_{2preamp} \end{bmatrix} \qquad [6]$$

and a noise contribution from each mouse and coil appears in each unfolded image. Since those noises are independent and will add in quadrature in the final images, the noise enhancement becomes significant as more mice are concurrently imaged.

In the case in which the coil shielding is complete, however, neither RF coil is sensitive to the other RF coil or mouse, so we only need to consider the noise in each

Table 2a
Mean $B_1$ Field Strength in a Shielded Birdcage Coil as a Percent of the Mean Field Strength in the Unshielded Coil

| Coil | Unshielded | Cylindrically shielded | Hexagonally shielded |
|---|---|---|---|
| 1 | 100 | 94 | 97 |
| 2 | 100 | 86 | 87 |
| 3 | 100 | 81 | 82 |

Table 2b
Root Mean Square Deviation in Percent of the $B_1$ Field Strength in an Unshielded Versus a Shielded Birdcage Coil

| Coil | Unshielded | Cylindrically shielded | Hexagonally shielded |
|---|---|---|---|
| 1 | 1.7 | 2.7 | 2.5 |
| 2 | 1.6 | 2.7 | 2.6 |
| 3 | 2.9 | 2.3 | 2.4 |

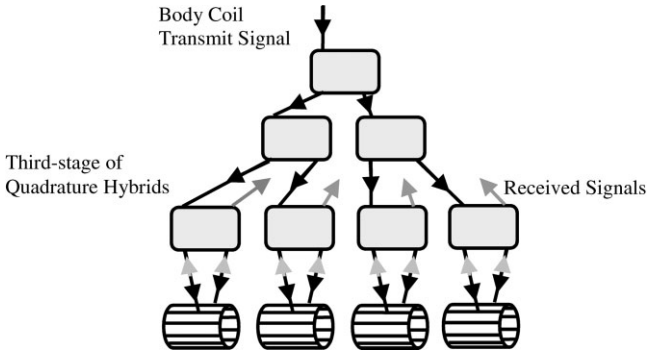


FIG. 6. An array of seven quadrature hybrids is used to split the transmit signal for the body coil (black arrows) into a quadrature transmit signal for each of four birdcage coils. During reception, the third stage of hybrids is used to combine the quadrature receive signals (gray arrows) from each coil for its receiver channel on the scanner.

received signal prior to coupling, $N_{1\mathrm{coil}} + N_{1\mathrm{mouse}}$ and $N_{2\mathrm{coil}} + N_{2\mathrm{mouse}} -$, provided that the coupling occurs before the preamplifier. After coupling, the noise in the first channel contains a sum of those two noises, weighted in the same manner as the signals, and the noise component from the second channel is completely correlated to the noise that was in that channel prior to coupling. Thus, we can write

$$\begin{bmatrix} N_1 \\ N_2 \end{bmatrix} = \begin{bmatrix} S_{11}(N_{11coil} + N_{11mouse}) + S_{12}(N_{12coil} + N_{12mouse}) + N_{1preamp} \\ S_{21}(N_{21coil} + N_{21mouse}) + S_{22}(N_{22coil} + N_{22mouse}) + N_{2preamp} \end{bmatrix}. \quad [7]$$

Signal separation with Eq. [4] yields

$$S_{i,j}^{-1}\mathrm{a} = \mathrm{v} + \begin{bmatrix} N_{1coil} + N_{1mouse} \\ N_{2coil} + N_{2mouse} \end{bmatrix} + S_{i,j}^{-1}\begin{bmatrix} N_{1preamp} \\ N_{2preamp} \end{bmatrix}; \quad [8]$$

therefore, the noise in each corrected image does not contain a noise component from either the other coil or its mouse, which is different from the noise result from generalized SENSE.

Thus, it is important that the RF coil shielding be as complete as possible in our multiple-mouse imaging experiment, although if we assume that preamplifier noise is negligible, then some cross-talk can be tolerated in the receiver electronics and can be corrected with no penalty in noise. However, complete isolation in all of the electronics would be ideal, because then no signal separation would be necessary.

To test our method of multiple-mouse imaging, we constructed an array of four shielded birdcage coils to use on our 1.5 T clinical scanner. We also performed bench-top experiments with two 300 MHz many-runged "Millipede" coils (20) to extend our observations from 1.5 T to 7 T.

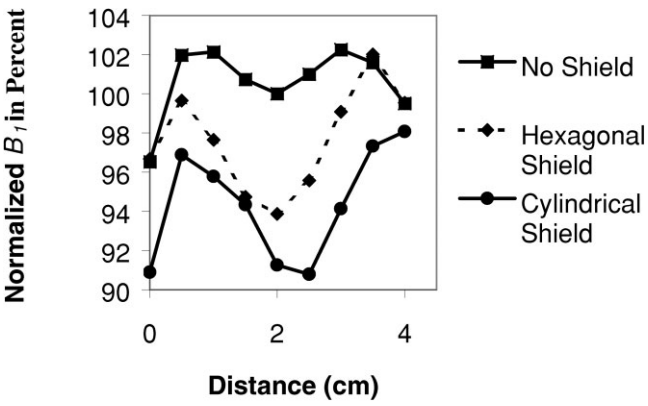


FIG. 5. A representative plot of the $B_1$ field strength along the centerline in birdcage coil #1 at 1.5T without shielding, or with a hexagonal or cylindrical shield. The field strength is presented as a percentage, normalized to its value at the center of the unshielded coil. Error bars for the repeat experiment are within the data symbols.

## Experimental Validation

We constructed four 16-rung, low-pass birdcage coils (3 cm diameter, 6 cm length) (21) from etched printed circuit board (40 μm copper thickness) and ceramic capacitors (American Technical Ceramics, Huntington Station, NY). We tuned and matched the coils to 63.85 MHz and 50 Ω, and placed cable chokes on their leads. Using 40-μm-thick copper foil, we built a set each of hexagonal (5 cm face-to-face, 20 cm length) and cylindrical (5 cm diameter, 20 cm length) grounded RF shields for the coils. We were able to operate the coils in quadrature using in-house-built lumped-element hybrids (22). We measured $Q$ based on the –3 dB bandwidth of the transmission between the orthogonal modes in empty hexagonally-shielded coils, and compared it to the $Q$ in coils loaded with a euthanized 25-g female CD-1 mouse (Charles River Laboratories, St. Constant, Quebec) to give the ratio of sample noise to coil noise at 1.5 T for mouse imaging. We repeated the measurements of $Q$ in two 300 MHz many-runged Millipede coils (Varian, Palo Alto, CA) designed for mouse imaging at 7 T.

Using the measurements of $Q_{\mathrm{loaded}}$ and $Q_{\mathrm{unloaded}}$, we found the ratio of mouse resistance ($R_{\mathrm{mouse}}$) to coil resistance ($R_{\mathrm{coil}}$) by the formula (23)

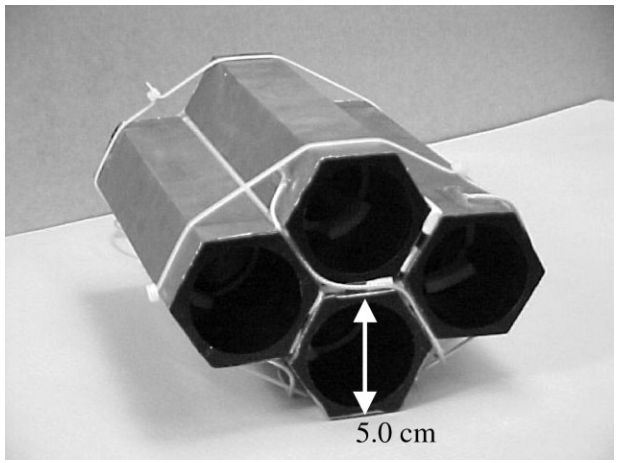


FIG. 7. An array of four birdcage coils in hexagonal shields for imaging at 1.5 T.

$$\frac{Q_{unloaded}}{Q_{loaded}} = \frac{R_{coil} + R_{mouse}}{R_{coil}}. \quad [9]$$

This allowed us to estimate the noise contribution from the mouse and the coil in Eq. [1]. In the four 63.85 MHz coils, $R_{\mathrm{mouse}}/R_{\mathrm{coil}}$ ranged between $3.0 \times 10^{-3}$ and $8.3 \times 10^{-3}$. In the two 300 MHz coils, $R_{\mathrm{mouse}}/R_{\mathrm{coil}}$ was 4.5 and 5.7, respectively. This suggests that at 1.5 T, coil noise in a mouse imaging experiment is dominating, while at 7 T, noise from the mouse is dominant.

Our hypothesis that the SNR in the *Mousehive* array could be increased by using hexagonal RF shields that pack in the magnet bore the same way that cylindrical ones would was based on the assumption that the greater mean shield diameter/coil diameter ratio in the hexagonal case would increase the $B_1$ sensitivity of each coil. To test this hypothesis, we compared $B_1$ field strength and homogeneity along the centerline of unshielded, cylindrically-shielded, and hexagonally-shielded coils driven in quadrature with a known voltage, using a 1-cm diameter pickup coil and a network/spectrum analyzer (Hewlett-Packard, Palo Alto, CA).

Table 2 shows measurements taken along the centerline in the central 4 cm of the coil of three of our birdcage coils for imaging at 1.5 T. Figure 5 shows a representative plot of the normalized field strengths in a coil with the two shield geometries. The mean $B_1$ value is the mean of the $B_1$ strength at 0.5-cm increments along the centerline of the coil with either a cylindrical shield or a hexagonal shield divided by the $B_1$ strength at the corresponding locations in the unshielded coil. The root mean square deviation in the $B_1$ field along the centerline of each coil and shield configuration is also presented as a measure of homogeneity.

We see from those results that there is a negligible increase in $B_1$ strength in going from a cylindrical shield to a hexagonal one, and that the homogeneity in $B_1$ is not adversely affected. However, since noise from the mouse will be dominating when we image at 7 T, Eq. [1] states that $B_1$ will not factor into the SNR, and there is no advantage in using the more complicated hexagonal shield geometry.

We next assembled a network of seven quadrature hybrids (Fig. 6) so that the four birdcage coils could be run simultaneously on a GE Signa CVMR clinical 1.5 T system with phased-array capabilities (GE Medical Systems, Milwaukee, WI). The transmit signal originally intended for the body coil was attenuated by 30 dB at the output of the RF signal generator, and the first and second stages of the hybrid network split it into four equal-amplitude voltage sources for a third stage of hybrids. The transmit signal was attenuated because the birdcage coils required significantly less power than the body coil for a 90° tip angle. We arranged the four hexagonally-shielded birdcage coils in a close-packed array (Fig. 7) and attached their leads to the third stage of hybrids to allow for transmission. The third stage of hybrids was also used for reception from the coils, and we connected the hybrids' receive ports to the four phased-array receiver channels on the scanner. We placed crossed diodes at the transmit ports of the third stage hybrids to improve isolation in the array.

Before we used that array for imaging, we investigated three main potential sources of signal interaction in the system: *1* electromagnetic interaction between the physi-

Table 3a
Isolation (dB) Between Physical RF Coils in the Multiple-Mouse Array

| Coil | 1 | 2 | 3 | 4 |
|---|---|---|---|---|
| 1 | | −56 ± 1 | −54 ± 2 | −55 ± 3 |
| 2 | −57 ± 2 | | −55 ± 3 | −60 ± 2 |
| 3 | −55 ± 3 | −56 ± 3 | | −57 ± 2 |
| 4 | −58 ± 2 | −60 ± 2 | −57 ± 3 | |

Table 3b
Isolation (dB) Between Images Made With a Single Coil on Each Parallel Receiver on the Scanner

| Image | 1 | 2 | 3 | 4 |
|---|---|---|---|---|
| 1 | | −30 ± 1 | −45 ± 5 | −32 ± 2 |
| 2 | −32 ± 1 | | −48 ± 5 | −43 ± 4 |
| 3 | −42 ± 5 | −41 ± 5 | | −25 ± 1 |
| 4 | −35 ± 1 | −42 ± 2 | −29 ± 1 | |

Table 3c
Total Isolation (dB) Between Images in the Multiple-Mouse Imaging Experiment

| Image | 1 | 2 | 3 | 4 |
|---|---|---|---|---|
| 1 | | −26 ± 1 | −38 ± 2 | −37 ± 2 |
| 2 | −24 ± 1 | | −45 ± 4 | −46 ± 6 |
| 3 | −43 ± 6 | −44 ± 1 | | −20 ± 1 |
| 4 | −38 ± 2 | −40 ± 1 | −19 ± 1 | |

Table 3d
Isolation (dB) Between Images After Post-processing

| Image | 1 | 2 | 3 | 4 |
|---|---|---|---|---|
| 1 | | −48 ± 6 | −48 ± 6 | −48 ± 6 |
| 2 | −52 ± 5 | | −50 ± 6 | −50 ± 5 |
| 3 | −47 ± 6 | −46 ± 6 | | −44 ± 5 |
| 4 | −46 ± 6 | −46 ± 6 | −41 ± 6 | |

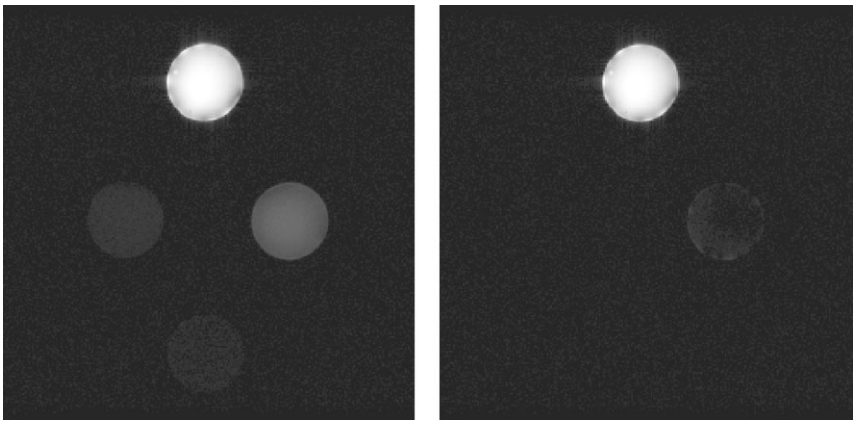

FIG. 8. Magnitude image showing ghosts from electronic interactions with other channels (left) and the same image following postprocessing (right).

cal RF coils, *2* interaction between the parallel receive channels on the scanner using a single coil, and *3* interaction between channels on the hybrid array. First, we measured isolation in the hexagonally shielded birdcage coils using the network analyzer to find the ratio of the output voltage at the receive port of the hybrid of one coil to the input voltage applied to the transmit port of the hybrid of any other coil. The shields were in direct mechanical, but not electrical, contact.

The isolation in dB between the 63.85 MHz hexagonally shielded RF coils is shown in Table 3a. An isolation of −54 dB between coils would mean that 0.2% of the signal voltage across one coil would be detected across a neighboring coil; hence, a 0.2% ghost artifact would appear in a magnitude image. Thus, we can see that the isolation in our shielded coils is excellent. The effectiveness of an RF shield is related to the skin depth of its material at the operating frequency, although care must be taken to ensure that the shield is not so thick that it interferes with the operating frequency of the gradients. No eddy-current artifacts were seen in images from our 63.85 MHz coils, indicating that the 40-μm copper foil was thick enough to block RF, but not so thick that it noticeably interfered with the gradients. At higher field strengths, the shielding can be made even thinner because skin depth is inversely proportional to frequency. This means that building effective RF shields should be even easier at higher field strengths. We repeated the isolation measurement in the 300 MHz coils and found the isolation between them to be 65 ± 3dB.

Next, we found the isolation between channels on the scanner by imaging a single birdcage coil loaded with a 25-g mouse phantom (2% agar, 2.5 g/l NaCl, 0.2 mM $MnCl_2$) on one of the scanner's phased-array ports. The other three ports were loaded with 50 Ω resistors (spoiled gradient-recalled echo (SPGR), TR/TE = 18/6.9 ms, flip angle = 30°, FOV = 14 cm, slice = 5 mm, frequency × phase = 256 × 256, NEX = 20). This produced four magnitude images: one from the channel loaded with the coil showing the phantom, and three from the resistor-loaded channels showing a ghost artifact. We found the isolation between channels from the magnitude images by drawing appropriate regions-of-interest (ROIs) and using

$$Isolation = 20 \log_{10}\langle I_i/I_j\rangle \qquad [10]$$

where $I_i$ is drawn in the phantom image for the $i^{\text{th}}$ image, and $I_j$ is drawn at the corresponding ghost artifact location of that phantom in the image from the $j^{\text{th}}$ channel. These images were divided pixel by pixel, and the mean pixel value of the resulting image was converted into dB for the isolation measurement. We also measured SNR in the phantom images to be used as the single coil reference case.

The isolation between images from parallel channels on the scanner that we measured is presented in Table 3b. There, the interaction between channels produced measurable ghosts.

Next, we found the total signal interaction in the system by imaging the four-coil array with an FOV that covered all of the coils (SPGR, TR/TE = 18/6.9 ms, flip angle = 30°, FOV = 14 cm, slice = 5 mm, frequency × phase = 256 × 256, NEX = 20). Once again, ghost images of the phantoms in the coils of other channels were seen in the magnitude images from each channel.

The isolation between the images from parallel channels in our complete arrangement is presented in Table 3c. In this arrangement the isolation was further compromised by cross-talk in the array of quadrature hybrids, and the worst ghost seen in a magnitude image was 11% of the primary image. These conditions may be tolerable in a four-channel system such as ours, since in a reduced FOV image, any mouse would only have three other mouse ghosts superimposed on it. In a system with more channels, however, those ghosts would seriously degrade image quality. Although it may be possible to improve the isolation in the electronics, we decided instead to postprocess the images to eliminate the ghosts. Since the RF coils had full shielding and were not sensitive to the phantoms in other coils, we were able to implement postprocessing with a sensitivity matrix that was the same for all pixels in the images and only needed to be measured once for the experimental setup.

We created a complex sensitivity matrix, *S*, from the complex image data by calculating

$$S_{i,j} = \langle I_i/I_j\rangle \qquad [11]$$

where $I_i$ was drawn in the phantom image from the $i^{\text{th}}$ channel and $I_j$ was drawn at the corresponding ghost artifact location of that phantom in the image from the $j^{\text{th}}$

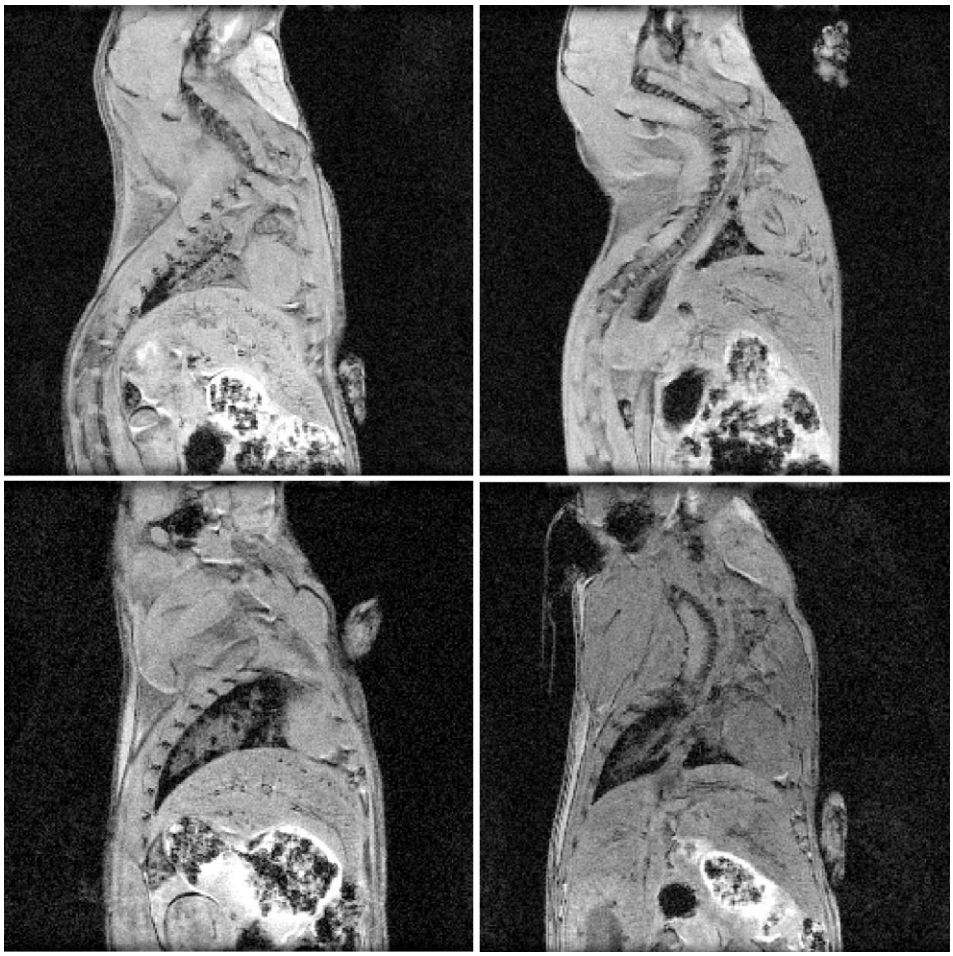

FIG. 9. One slice from each of four 3D mouse images simultaneously acquired.

channel Those images were divided pixel by pixel, and the mean pixel value of the resulting image was used for *S*.

We calculated the inverse complex sensitivity matrix using Gaussian elimination in Matlab (Mathworks, Natick, MA) and corrected the images. As before, we drew ROIs in the images, and calculated the isolation between the channels.

Table 3d shows the final isolation between images from parallel channels measured in the postprocessed images, and Fig. 8 shows the corrected image from the fourth channel. After processing, our final worst-magnitude image ghost was only 0.9%.

We calculated the SNR in the original and postprocessed images. Since the pulse sequence was the same one used to image the single coils, we could make an SNR comparison between a single coil and four coils together.

In terms of efficiency, the SNR in the four multicoil images was 0.98–1.11 times greater than that in the single-coil images, demonstrating that the two cases had comparable SNRs. However, the multicoil images were acquired in a quarter of the total time; thus, the efficiency was four times better than the efficiency in the single-coil case, as predicted in our theory. The SNR in the postprocessed multicoil images was 0.96–1.00 of its prior value, suggesting that the SNR was not significantly affected by our postprocessing method.

Finally, to demonstrate reduced-FOV imaging, we imaged four euthanized female CD-1 mice using the array. We used a 2D sequence (SPGR, TR/TE = 39/12.9 ms, flip angle = 30°, FOV = 13 cm, slice = 0.8 mm, frequency × phase = 256 × 256, NEX = 30) with an FOV covering all of the mice in the array to determine the sensitivity matrix. For high-resolution mouse imaging, we used a 3D sequence (SPGR, TR/TE = 56/10 ms, flip angle = 30°, FOV = 4 cm × 4 cm × 4.2 cm, frequency × phase × phase = 256 × 256 × 60, NEX = 4) with the phase-encoding gradients across the face of the array. We set the FOV over only the first mouse in the array and the other mice were spatially encoded by replicated FOVs. We postprocessed those images using the sensitivity matrix data from the first sequence and corrected the FOV centers in the phase-encoding directions.

Figure 9 shows postprocessed sagittal images from our 3D multiple-mouse imaging experiment. The four mouse images were acquired in about 1 hr, compared to the 4 hr they would have taken if acquired individually. The postprocessed images show negligible ghosting artifact and the mice are centered in their replicated FOVs.

## CONCLUSIONS

We have achieved a significant improvement in efficiency in a whole-body 3D multiple-mouse imaging experiment

using an array of shielded birdcage coils. Such coils are commercially available, and the trend toward using more parallel receiver channels on modern scanners means that our method can be readily implemented. One could also improve upon the isolation in the electronics, perhaps to the point where postprocessing would be unnecessary. Our postprocessing method is quite simple to use since we need only one measurement of sensitivity for all pixels in the image, and this measurement only has to be performed once for the electronics used in an experiment. We have also demonstrated that good isolation is obtained in RF coils at 1.5 T and at 7 T, suggesting that our method will be practical at higher fields. Overall, our findings demonstrate that increased imaging efficiency is possible with multiple-mouse MRI.

## REFERENCES


1. Nadeau JH, Balling R, Barsh G, Beier D, Brown SDM, Bucan M, Camper S, Carlson G, Copeland N, Eppig J, Fletcher C, Frankel N, Ganten D, Goldowitz D, Goodnow C, Guenet J, Hicks G, Hrabe de Angelis M, Jackson I, Jacob HJ, Jenkins N, Johnson D, Justice M, Kay S, Kingsley D, Leharch H, Magnuson T, Meisler M, Poustka A, Rinchik EM, Rossant J, Russell LB, Schimenti J, Shiroishi T, Skarnes WC, Soriano P, Stanford W, Takahashi JS, Wurst W, Zimmer A. Functional annotation of mouse genome sequences. Science 2001;291:1251–1255.
2. Brown SDM, Balling R. Systematic approaches to mouse mutagenesis. Curr Opin Genet Dev 2001;11:268–273.
3. Johnson GA, Cofer GP, Gewalt SL, Hedlund LW. Morphologic phenotyping with MR microscopy: the visible mouse. Radiology 2002;222: 789–793.
4. Streicher J, Weninger WJ, Muller GB. External marker-based automatic congruencing: a new method of 3D reconstruction from serial sections. Anat Rec 1997;248:583–602.
5. Thévenaz P, Ruttiman UE, Unser M. A pyramid approach to subpixel registration based on intensity. IEEE Trans Image Processing 1998;7: 27–41.
6. Hedlund LW, Fubara B, Cofer GP, Kelly SJ, Gewalt SL, Hershfield MS, Johnson GA. Morphologic phenotyping of a uricase knockout using MR microscopy of fixed/stained whole specimens. In: Proceedings of the 9th Annual Meeting of ISMRM, Glasgow, Scotland, 2001. p 926.
7. Brown SDM, Nolan PM. Mouse mutagenesis—systematic studies of mammalian gene function. Hum Mol Genet 1998;7:1627–1633.
8. Li Y, Wolters AM, Malawey PV, Sweedler JV, Webb AG. Multiple solenoidal microcoil probes for high-sensitivity, high-throughput nuclear magnetic resonance spectroscopy. Anal Chem 1999;71:4815–4820.
9. Fisher G, Petucci C, MacNamara E, Raftery D. NMR probe for the simultaneous acquisition of multiple samples. J Magn Reson 1999;138: 160–163.
10. Rossman P, Reiderer S, Hulshizer T, Felmlee J, Kruger D. Use of independent transmit/receive coils for reduction of acquisition time in imaging of the legs. In: Proceedings of the 10th Annual Meeting of ISMRM, Honolulu, 2002. p 869.
11. Wright SM, McDougall M, Brown DG, Hazle J. Arrays of birdcage coils for imaging multiple samples. In: Proceedings of the 9th Annual Meeting of ISMRM, Glasgow, Scotland, 2001. p 18.
12. Kose K, Haishi T, Matsuda Y, Anno I. Super-parallel MR microscope. In: Proceedings of the 9th Annual Meeting of ISMRM, Glasgow, Scotland, 2001. p 609.
13. Morris HD, Chesnik S. Two methods for multi-sample imaging: applications to mouse phenotyping via MRI. In: Proceedings of the 9th Annual Meeting of ISMRM, Glasgow, Scotland, 2001. p 19.
14. Bock NA, Konyer NB, Henkelman RM. Multiple-Mouse MRI. In: Proceedings of the 9th Annual Meeting of ISMRM, Glasgow, Scotland, 2001. p 1108.
15. Hoult DI, Lauterbur PC. The sensitivity of the zeugmatographic experiment involving human samples. J Magn Reson 1979;34:425–433.
16. Porter JR, Wright SM, Famili N. A four-channel time domain multiplexer: a cost-effective alternative to multiple receivers. Magn Reson Med 1994;32:499–504.
17. Graham RL, Lubachevsky BD, Nurmela KJ, Östergård PRJ. Dense packings of congruent circles in a circle. Discrete Math 1998;181:139–154.
18. Collins CM, Li S, Yang QX, Smith MB. A method for accurate calculation of $B_1$ fields in three dimensions. Effects of shield geometry on field strength and homogeneity in the birdcage coil. J Magn Reson 1997;125: 233–241.
19. Pruessmann KP, Weiger M, Scheidegger MB, Boesiger P. SENSE: sensitivity encoding for fast MRI. Magn Reson Med 1999;42:952–962.
20. Wong WH, Sukumar S. "Millipede" imaging coil design for high field micro imaging applications. In: Proceedings of the 8th Annual Meeting of ISMRM, Denver, 2000. p 1399.
21. Hayes CE, Edelstein WA, Schenck JF, Mueller OM, Eash M. An efficient, highly homogenous radiofrequency coil for whole-body NMR imaging at 1.5 T. J Magn Reson 1985;63:622–628.
22. Sorgenfrei BL, Edelstein WA. Optimizing MRI signal-to-noise ratio for quadrature unmatched RF coils: two preamplifiers are better than one. Magn Reson Med 1996;36:104–110.
23. Wright CA, Song HK, Wehrli FW. In vivo MR micro imaging with conventional radiofrequency coils cooled to 77°K. Magn Reson Med 2000;43:163–169.